ACS SENSORS

pubs.acs.org/acssensors

Article

Design and Implementation of a Dual-Region Self-Referencing Fiber-Optic Surface Plasmon Resonance Biosensor

Valentina Bello, Wouter Vandezande, Devin Daems, and Jeroen Lammertyn*

Cite This: *ACS Sens.* 2022, 7, 3360−3368

Read Online

ACCESS | Metrics & More | Article Recommendations | Supporting Information

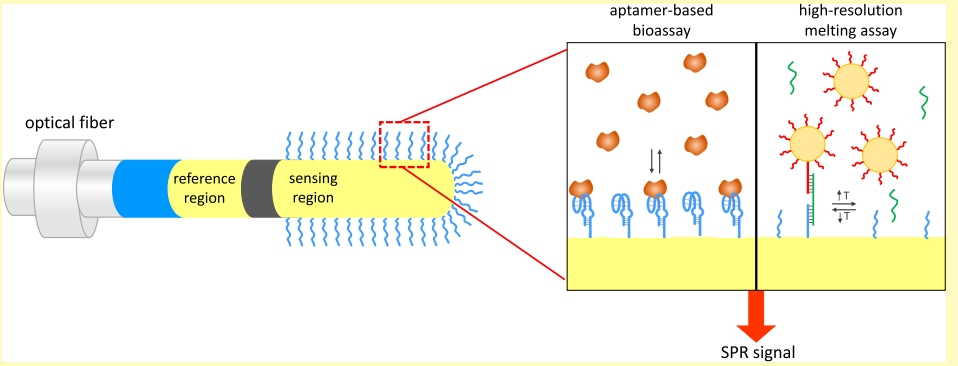

ABSTRACT: The need for self-referencing is extremely important in the field of biosensing. In this manuscript, we report on the study, design, and validation of a dual-region self-referencing fiber-optic surface plasmon resonance biosensor. One region is intended to measure and monitor the binding events of the biological sample under test, while the other one is designed to be used as a reference channel to compensate for external factors, such as bulk refractive index modifications and temperature oscillations, that can negatively affect the biomolecular interaction measurement. Two different configurations for the biosensor probe are presented and investigated here, both theoretically and experimentally. First, the theoretical performance of the proposed biosensor probes, in terms of surface plasmon resonance wavelength shift, was simulated using a numerical model. Afterward, they were experimentally validated in sucrose−water solutions and showed a response to refractive index and temperature changes with sensitivities up to 2000 nm/RIU and 1.559 nm/°C, respectively. Finally, an aptamer-based bioassay and a high-resolution melting assay were successfully implemented on the two proposed configurations, demonstrating the feasibility of analyzing the binding events and measuring other external signal modifications simultaneously using the same biosensor probe.

KEYWORDS: *surface plasmon resonance, fiber-optic biosensor, dual-region biosensor, aptamer-based bioassay, high-resolution melting assay*

During the last decades, surface plasmon resonance (SPR) has established itself as an extremely powerful optical sensing technique with important applications in the fields of medical diagnostics, food safety, life science, and environmental monitoring.[1−4] In particular, plasmonics is the study of the interaction between optical-frequency electromagnetic field oscillations and free electrons in a metal.[5] Because of the resonant coupling with photon momentum, the free electrons undergo collective oscillations called plasmon waves or surface plasmons (SPs). The SPs can be excited at the interface between a metal (such as gold, silver, chromium, or titanium), generating an evanescent wave whose electric field penetrates both surrounding media. The evanescent field is strongly enhanced in the proximity of the interface, and it can be applied to sense the refractive index (RI) close to the metal surface, where the molecular binding events take place. The RI increase produces an increase in the propagation constant of SPs traveling along the metallic surface that can be optically measured.[6]

Nonetheless, traditional SPR sensing solutions, which are mainly based on dielectric prisms,[7] are rarely used outside research laboratories because they are expensive, bulky, and usually require a complex microfluidic circuit for the handling of samples.[8,9] These drawbacks can be overcome using fiber-optic surface plasmon resonance (FO-SPR) sensors, which turn out to be particularly suitable for biomedical sensing applications. Indeed, FO-SPR biosensing platforms allow label-

Received: June 27, 2022
Accepted: October 14, 2022
Published: October 21, 2022

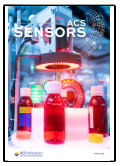

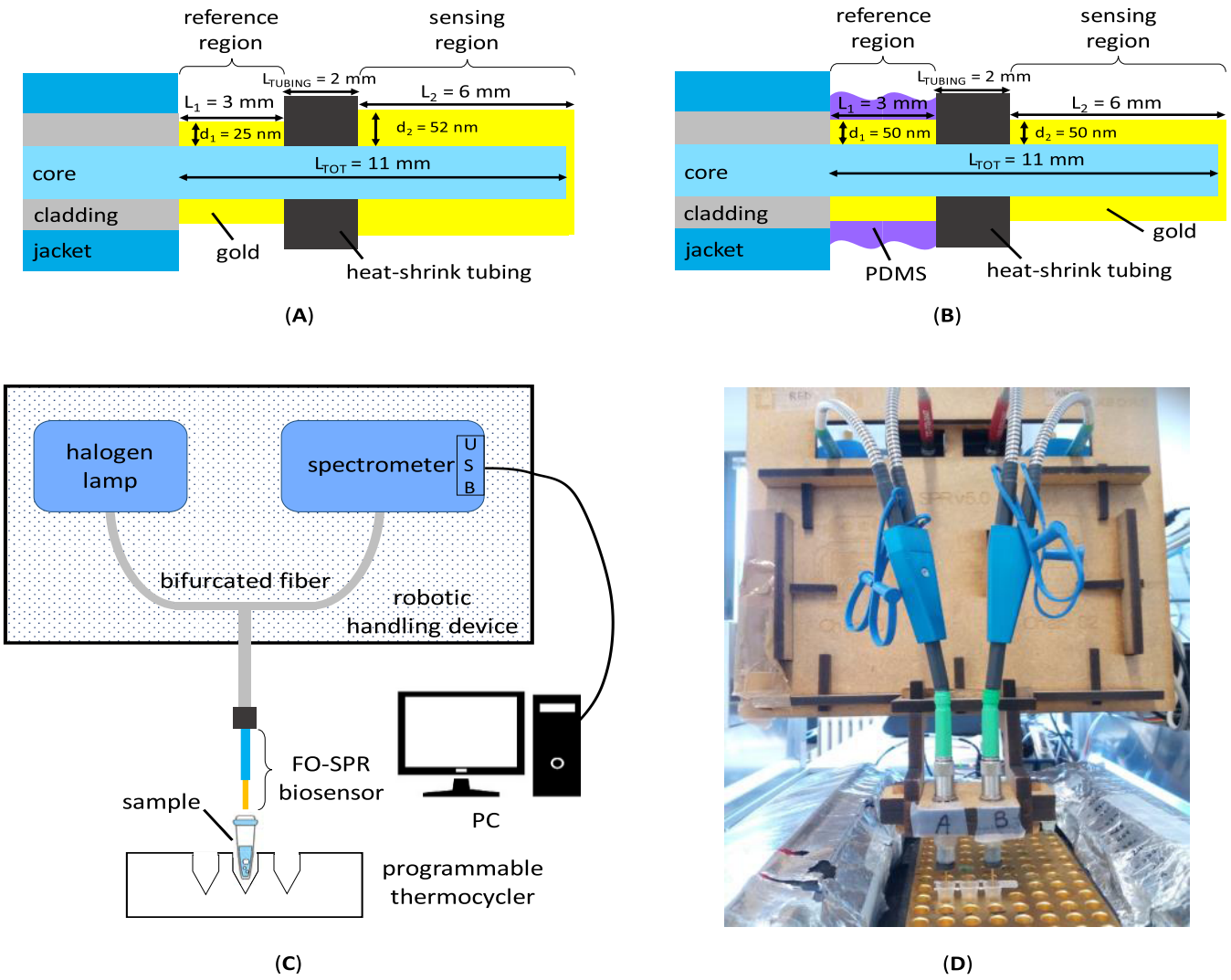

Figure 1. Schematics of the proposed FO-SPR probe configurations and instrumental setup. (A) The gold−gold probe configuration is characterized by two separate regions with different gold thicknesses divided by a short segment of heat-shrink tubing. (B) The PDMS−gold probe configuration features an extra PDMS layer deposited on the reference region for the detection of sample temperature. (C) Experimental setup: light produced by a halogen lamp reaches the sensing tip through a bifurcated fiber. The spectrum of the back-reflected light is reconstructed via a spectrometer USB connected to a computer that allows data acquisition. (D) Picture of the actual laboratory configuration featuring a double setup (two lamps, two spectrophotometers, two bifurcated fibers, and two biosensor tips).

free and real-time detection of biological binding reactions, resulting in a compact and cost-effective sensing tool. Moreover, they also feature the possibility of improving sensitivity through the incorporation of nanoparticles (NPs) into bioassays.[10−12]

Nevertheless, when using FO-SPR-based sensors and biosensors, a critical issue is represented by the need for self-referencing. Indeed, the SPR signal can be affected not only by the variation of the parameter under study but also by external factors, such as modifications of the bulk RI of the surrounding medium and, in particular, temperature fluctuations. By using a biosensor provided with a single sensing region, it is not possible to distinguish between the signal actually produced by the variation of the parameter under study and the changes induced by the factors previously listed. Several research groups have proposed solutions in the literature to tackle this issue. For example, many works rely on the use of single-mode fiber (SMF) gratings. Li et al. proposed an implantable FO-SPR biosensor for continuous glucose monitoring[13] in which the sensing region was coated with chromium and gold layers and afterward covered with a semipermeable polymeric PAA-ran-PAAPBA membrane to suppress the measurement interference of other substances. Moreover, a long-period fiber grating was written into the fiber core to compensate for body temperature drift that had a big effect on the measurement results. Liu et al. proposed an s-tilted fiber Bragg grating SPR (TFBG-SPR) sensor to discriminate between bulk and surface-localized RI changes.[14] Such discrimination is enabled by the differential sensitivities of the hybrid plasmon modes and near-cutoff modes of the TFBG-SPR sensor. Garg et al. reported an SPR sensor based on SMF long-period gratings.[15] They achieved a double-resonance response by introducing an optical path difference between the core and cladding modes and demonstrated a simultaneous measurement of the refractive index and temperature. Hu et al. realized an SPR sensor constituted of two multimode fibers and an SMF Bragg grating, which is spliced in between them, coated with a silver film.[16] They

https://doi.org/10.1021/acssensors.2c01362
ACS Sens. 2022, 7, 3360−3368

demonstrated RI and temperature measurements, with sensitivities of 2556.8 nm/RIU and 172 pm/°C, respectively. These sensors are surely interesting solutions but usually require a complex fabrication process and expensive extra components (polarization controllers and couplers). Moreover, currently, their operation has not been experimentally proved with biological sensing and bioassays. Other types of FO-SPR solutions have also been proposed to address the matter of self-referencing. Weng et al. presented a complex double-sided polished fiber coated with gold and silver for the simultaneous measurements of RI and temperature, exploiting the resonance wavelengths of the *x*- and *y*-polarized loss spectra.[17] Velázquez-González et al. realized a dual-region SPR-FO sensor for simultaneous measurements of RI and temperature by inserting a section of single-mode fiber between two multimode fibers.[18] The single-mode fiber was coated with a layer of chromium and gold and then half of its length was covered with polydimethylsiloxane (PDMS). Good levels of sensitivity were achieved, but the deposition method of the PDMS used in this work did not allow having a precise control of the length of the two sensing regions and, thus, on the position of the resonance wavelengths. In another interesting paper,[19] Peng et al. described a dual-channel FO-SPR sensor based on the deposition of a polymer matrix of poly-(allylamine-hydrochloride) in which both channels were sensitive to RI and temperature variations. Another recent paper presented a complex optical fiber DNA hybridization sensor based on SPR combined with interferometry for temperature compensation.[20] Other self-referencing FO-SPR biosensors featuring complex structures and polymeric or dielectric overlayers were presented and based on mixed detection methods in the literature.[21−28]

Despite the recent advances in self-referencing optical fiber sensors, there is still a need for reliable, robust, and low-cost technological solutions that ensure a good level of sensitivity but without requiring complex and expensive micromachining fabrication techniques. Moreover, to the best of our knowledge, only very few of the presented FO-SPR biosensors with self-referencing system have been actually exploited yet to test biological samples or perform bioassay analyses. In this study, we propose a self-referencing dual-region FO-SPR biosensor, with two different configurations of the fiber probe, as a solution to the issue of compensation for factors that can affect the FO-SPR signal. The first one (gold−gold configuration) consists of two regions of different lengths coated with gold layers of different thicknesses separated by a small heat-shrink tubing of polymeric material (Figure 1A). It can be employed to compensate for bulk RI modifications, and it was exploited in the implementation of an aptamer-based bioassay for α-thrombin detection. The second configuration (PDMS−gold configuration) includes an extra PDMS coating on just one region and is designed to monitor temperature variations (Figure 1B). To realize the innovative FO-SPR probe configurations, only a few extra fabrication steps are required with respect to a traditional FO-SPR biosensor. However, a little extra complexity level is worth in order to a single biosensor that integrates both referencing and sensing functions in one single device. As a proof of concept, the second configuration is successfully used to perform a high-resolution DNA melting (HRM) assay. Both configurations work in a reflection mode since the gold layer deposited on the fiber tip acts as a mirror, back-reflecting light that crosses twice the two regions. To better understand the performance of the dual-region FO-SPR biosensors as a function of RI and temperature variations, a theoretical model is implemented following the theory on optical waves in isotropic layered media. For the first time to the best of our knowledge, this work shows how the same FO-SPR biosensor can successfully combine the possibility of performing DNA-based bioassays with simultaneous integrated temperature monitoring, both based on the SPR detection technique. Moreover, the experimental data are confirmed by an accurate and reliable theoretical and modeling background.

MATERIALS AND METHODS

Design and Fabrication of the FO-SPR Probe Configurations. The protocol for the fabrication of the FO-SPR biosensors consists of two main steps: the preparation of the optical fiber and the deposition of the plasmonic metal layer. FT400EMT TEQS multimode fiber (Thorlabs, Newton, NJ) with a core diameter of 400 μm and a numerical aperture of 0.39 was used. To prepare each FO-SPR probe, a 16 cm long piece of fiber was cut. Afterward, the initial and final parts of the jacket were stripped off and the TEQS hard polymer cladding was removed using acetone and lens cleaning tissues. The two extremities of the fiber were cleaved with a fiber cleaver (LDC400, Vytran, Morganville, NJ) to get perfectly flat ending facets. Eventually, the metal layers were sputtered on the fiber core by vapor phase deposition with a Q150T ES machine (Quorum Technologies, Lewes, U.K.). Gold was chosen for the coating since it is biocompatible, chemically stable, and resistant to oxidation. Two FO-SPR probe configurations were designed and fabricated. The gold−gold configuration (Figure 1A) consisted of two regions with lengths L_1 = 3 mm and L_2 = 6 mm, respectively. The two segments were sputtered with gold layers of different thicknesses, d_1 = 25 nm and d_2 = 52 nm, respectively. The amount of metal deposited during the process was controlled by means of a quartz film thickness monitoring crystal located inside the sputtering chamber. To physically divide the sensing and reference regions and better distinguish them during the functionalization process, a short piece of heat-shrink tubing was inserted between them. The length of the separation element was L_{TUBING} = 2 mm, so that $L_{TOT} = L_1 + L_{TUBING} + L_2$ = 11 mm. The PDMS−gold configuration was designed to compensate for unwanted variations of the SPR signal caused by temperature oscillations. As shown in Figure 1B, the geometrical dimensions were L_1 = 3 mm, L_{TUBING} = 2 mm, L_2 = 6 mm, and $d_1 = d_2$ = 50 nm. Moreover, the reference region was coated with an extra PDMS layer after the gold deposition step. PDMS was chosen because it is biocompatible, chemically inert, and nontoxic, thus being suitable for biosensing. Moreover, it exhibits a high thermo-optic coefficient (TOC), given by $k = \partial n/\partial T = -4.5 \times 10^{-4}$ RIU/°C,[29] where n is the refractive index and T is the temperature (°C). The negative sign of the TOC refers to a decreasing RI of PDMS with increasing temperature. The polymeric mixture was prepared by mixing a Sylgard 184 silicon elastomer (Dow Corning, Midland, MI) and a curing agent in a ratio of 10:1. The mixture was inserted in the desiccator for 10 min to remove all air bubbles. Then, the polymer was deposited on the gold-coated reference region using a small brush and the FO-SPR biosensor was inserted in the oven at 150 °C for 30 min for the curing step. It is important to stress that a perfect control of the thickness of the PDMS layer was not necessary. It was only required that the polymeric layer was thicker than the penetration depth of the evanescent wave to ensure that the SPR signal corresponding to the reference region was affected only by thermal effects and not also by RI variations of the sample under test. The thickness of the PDMS layer deposited here was in the order of 1−2 mm.

Theoretical Model. To better understand the performances of the dual-region FO-SPR biosensors, a theoretical model was implemented in MATLAB (MathWorks, Natick, MA) code following the theory on optical waves in isotropic layered media presented by Pochi Yeh[30] and on SPR in optical fibers.[31,32] For each FO-SPR probe

https://doi.org/10.1021/acssensors.2c01362
ACS Sens. 2022, 7, 3360−3368

configuration, the spectral response of the overall FO-SPR biosensor was obtained by multiplying the spectral response of the sensing region and of the reference region, each considered as being the only region present on the fiber-optic probe.[33] Theoretical simulations were carried out to predict the effect of different lengths of the two regions, different thicknesses of the metal layers, and the deposition of extra polymeric layers on the wavelength position of the SPR resonances. Moreover, the model was also used to simulate the spectral response of the FO-SPR probes when dipped in samples with different RIs and to extract the theoretical calibration curves and sensitivities. Eventually, the model was exploited to predict and explain the variability in the actual responses among different probes. Indeed, producing two perfectly identical FO-SPR probes was not feasible: as a consequence, the spectrum profile and the sensitivity can slightly differ from one probe to the other. More detailed information about the implementation of the theoretical model and its use to study the FO-SPR biosensor variability can be found in the Supporting Information.

Experimental Setup. The instrumental configuration employed to perform experimental measurements is reported in Figure 1C. The source was a tungsten halogen lamp HL-2000-FHSA (Ocean Optics, Largo, FL), with an emission in the range from 360 to 2400 nm. The broad-band light was coupled into a bifurcate fiber connected with the biosensor by means of a SubMiniatur version A (SMA) connector. Incident light excited the plasmonic wave at the interface between the gold layer and the sample solution. The light crossing the sensing zone was back-reflected by the distal mirror and coupled into the second arm of the bifurcated fiber before being collected by a spectrophotometer with a detection range from 350 to 1100 nm (USB4000, Ocean Optics, Largo, FL). The setup was attached to a computer-controlled robot (Colinbus, Hulshout, Belgium) to ensure a fully automated handling. Moreover, a programmable thermocycler (Westbur, Leusden, The Netherlands) was used to control and set the temperature during the HRM assay. Figure 1D shows a picture of the laboratory instrumentation attached to the robot, featuring a double setup (thus with two lamps, two spectrophotometers, two bifurcated fibers, and two biosensor tips) to carry out two tests simultaneously.

Aptamer-Based Bioassay for α-Thrombin Detection. The gold−gold probe configuration was tested with an aptamer-based bioassay for the detection of the concentration of human α-thrombin,[34] an important protein that takes part in the process of blood coagulation. The FO-SPR biosensor probes were functionalized using DNA aptamers with sequence 5′-AGT CCG TGG TAG GGC AGG TTG GGG TGA CT-3′.[35] The thiolated probes (50 μL, 100 μM) were first reduced with 50 μL of 0.1 M dithiothreitol (DTT) (in phosphate buffer (PB) 0.18 M, pH 8.3). DTT was used to separate thiol dimers that could lower the efficiency of the functionalization process. After 1 h of incubation, the solution was purified with a GE NAP 5 column (Ge Healthcare, Chicago, IL); 10 mM Tris and 1 mM ethylenediaminetetraacetic acid (EDTA)—(TE) buffer were used to rinse the column five times and to elute the purified DNA dropped out from the column after purification. DNA incubation solution (150 μL) was prepared by mixing 18 μL of 1 μM DNA reduced aptamers, 37.5 μL of 4 M NaCl in 0.01 M PB + 0.01% sodium dodecyl sulfate (SDS) (pH 8), and 94.5 μL of 0.01 M PB + 0.01% SDS. The freshly sputtered optical fiber sensing probes were placed inside the solution and incubated overnight at 4 °C. The sensing region was functionalized by carefully dipping only the distal end of the sensing probes in the solution. The day after, the FO-SPR biosensors (both reference and sensing regions) were backfilled with poly(ethylene glycol) (PEG) to avoid nonspecific binding. Hereto, a PEG solution was prepared by dissolving 1 μL of 5 mM PEG in 500 μL of absolute ethanol. The PEG solution was diluted in tris(hydroxyamino)-methane-glycine-potassium (TGK), bovine serum albumin (BSA), and Tween 20 buffer, and fibers were incubated in this mixture at 4 °C for 1 h. After a final washing step, the FO-SPR biosensors were stored at 4 °C in TGK−BSA−Tween 20 buffer until further use. A human α-thrombin (Bio-Connect, Huissen, The Netherlands) dilution series (0, 62, 124, 248 nM) was prepared in TGK−BSA−Tween 20 buffer. For every tested concentration, the bioassay cycle consisted of four consecutive steps: (i) washing in TGK−BSA−Tween 20 buffer for 180 s; (ii) immersion in the α-thrombin sample for 1200 s; (iii) washing in TGK−BSA−Tween 2o buffer for 180 s; (iv) regeneration in regeneration buffer (1 M NaCl in 50 mM NaOH) for 30 s.

High-Resolution Melting Assay. A HRM assay was implemented on the PDMS−gold probe configuration. Here, gold NPs (Au NPs) were employed for signal amplification and improvement of the bioassay sensitivity.[36] Three DNA sequences were used: two for functionalization of NPs and the optical fiber surface, respectively, and one as target molecule (Figure 4A). The same protocol presented in a previous work was followed.[37] Au NPs with an average diameter of 20 nm (BBI Solutions, Cardiff, U.K.) were functionalized with *Mtd*3 5′ thiol probe (5′-thiol MC6-D/TTT TTT TTT TGC TGA CTC AT). Fifty microliters of 100 μM DNA were first activated with DTT (0.1 M in PB 0.18 mM, pH 8.3). The solution was incubated for 1 h at room temperature. Subsequently, the DTT was removed by DNA purification through a GE NAP 5 column, following the same procedure previously described. Two hundred microliters of the reduced 1 μM DNA solution were then added to 2 mL of 50 μM Au NPs. Consequently, an accelerated salt maturation protocol was employed to maximize the DNA density on the NPs by adding increasing volumes of 4 M NaCl in PB-SDS. In the end, the NPs were incubated overnight at room temperature in a rotator. The day after, they were washed three times in PB + 0.01% SDS and PEG-backfilled. Eventually, the NP concentration was adjusted to a value of 2.32 nM by eluting them in nuclide-free (NF) water and measuring with a spectrophotometer. The FO-SPR biosensors were functionalized with *Mtd*3 3′ thiol probe (5′-GTG ACT CAG CAT GTA ATA TAT ATC TCA), following the same protocol used for functionalization of optical fibers already mentioned. The DNA incubation solution was prepared by mixing 40 μL of reduced DNA from the column, 83 μL of 4 M NaCl in PB-SDS, and 208 μL of PB-SDS. After overnight incubation, the FO-SPR biosensors were PEG-backfilled, washed, and stored in PB-SDS at 4 °C until further use. As better described in previous works,[11,37] each HRM cycle consisted of three steps during which the sample underwent different temperature conditions: (1) denaturation (5 min at 94 °C), (2) hybridization (15 min at 55 °C), and (3) melting (5 min at 94 °C with an increasing temperature coefficient of 0.1 °C/s). Two different kinds of samples were prepared to run the HRM assay: (i) blank solution, composed of 15 μL of NF water, 42 μL of PBS + 300 mM NaCl, and 43 μL of Au NPs in the absence of the target DNA sequence; (ii) reaction mixture, composed of 15 μL of Mtd3 (5′-CCC GTA CGA GAT ATA TTT TTG TCT GGT) target DNA (10 nM final concentration), 42 μL of PBS + 300 mM NaCl, and 43 μL of Au NPs. The liquids under study were covered with a layer of mineral oil to prevent evaporation during thermocycling.

Data Processing. The output spectra from the FO-SPR biosensors were acquired via a specifically designed LabVIEW (National Instruments, Austin, TX) interface that allowed us to monitor the spectral response of the biosensor and to acquire and visualize the sensorgram of the measurements in real time. Furthermore, a MATLAB code was written to process data after their acquisition. First, a moving average filter was applied to reduce the noise level in the data. Second, each spectrum was normalized to a reference spectrum acquired in air. Afterward, the SPR spectral resonances were fitted with a fourth-order polynomial function to find their wavelength position. Average values and standard deviations were calculated on the resonance wavelength positions of five different spectra (for each sample), obtained after polynomial fitting of the spectral minima. Lastly, the linear calibration curves were obtained by fitting the position of SPR resonances as a function of the sample RI.

RESULTS AND DISCUSSION

Theoretical Investigation and Experimental Testing of Gold−Gold Probe Configuration. The theoretical model previously described was used to simulate the FO-SPR

https://doi.org/10.1021/acssensors.2c01362
ACS Sens. 2022, 7, 3360−3368

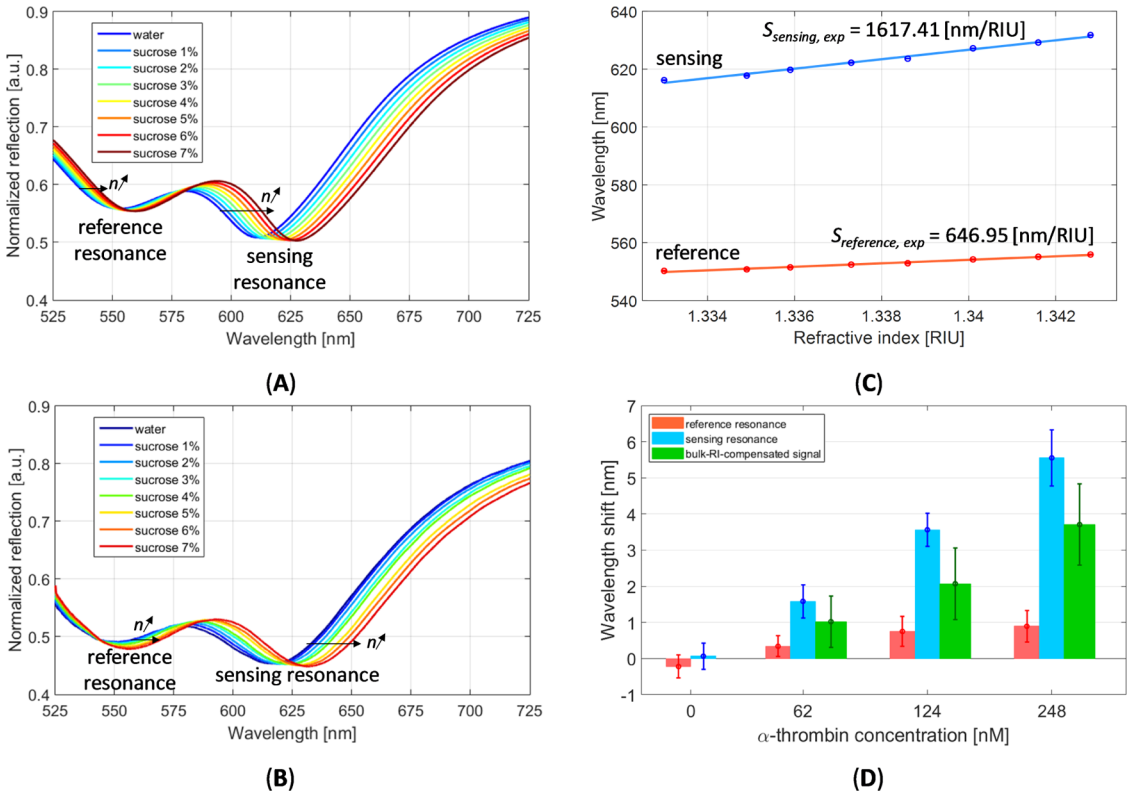

Figure 2. Theoretical and experimental results for the gold−gold probe configuration. (A) Theoretical output spectra: resonance positions shift toward higher values for increasing sample RI. (B) Experimental output spectra. (C) Experimental linear calibration curves for sensing and reference regions: error bars indicate 1 standard deviation (number of samples = 5). (D) Human α-thrombin bioassay results: the orange bars represent the reference resonance shift because of bulk RI variations; the light-blue bars represent the shift of the sensing resonance because of the binding events (aptamer−thrombin) taking place at the surface of the sensing region; the green bars refer to the bulk-RI-compensate signal obtained by subtraction of the reference wavelength shift from the sensing wavelength shift after sensitivity renormalization. Error bars indicate 1 standard deviation (number of samples = 5).

biosensor spectral response to sucrose−water solutions with RI varying from 1.3330 to 1.3432 RIU. The following geometrical dimensions were considered as input parameters for the model: L_1 = 3 mm, L_2 = 6 mm, d_1 = 25 nm, and d_2 = 52 nm. The theoretical spectra are reported in Figure 2A. Their shape is characterized by two minima, corresponding to the SPR resonances generated by the two probe regions: the first minimum (the "reference resonance"), located at 553.0 nm (in water), has to be ascribed to the reference region, while the second minimum (the "sensing resonance"), located at 610.8 nm (in water), is produced by the reference region. By linear fitting of the wavelength position of the resonances as a function of the sample RI, the theoretical linear calibration curves were retrieved, obtaining the theoretical sensitivities that correspond to the absolute values of the slopes of the calibration curves: $S_{reference,\ theor}$ = 646.95 nm/RIU and $S_{sensing,\ theor}$ = 1617.41 nm/RIU. Following the theoretical analysis, the FO-SPR biosensor was experimentally tested in sucrose−deionized water solutions in concentrations from 0 to 7 w/w %, corresponding to RI from 1.3330 to 1.3432 RIU. Figure 2B shows the experimentally obtained spectra. The wavelength position of the minima is in good agreement with the expected theoretical results: the reference resonance is located at 551.6 nm, while the sensing resonance occurs at 615.4, in water, and the experimental calibration curves, reported in Figure 2C, demonstrate that the experimental sensitivities ($S_{reference,\ exp}$ = 702.67 ± 0.52 nm/RIU and 1 $S_{sensing,\ exp}$ = 1653.86 ± 0.47 nm/RIU) fall in the range of the values predicted by the theoretical model (see the Supporting Information, Table S1 that lists the theoretical sensitivity values for varying values of the design geometrical parameters).

As a proof of concept, the bioassay for α-thrombin detection was implemented by functionalizing only the sensing region. The reference region was intentionally not functionalized as it was intended as the reference channel to sense possible bulk RI variations occurring in the sample. Indeed, it is reasonable to assume that no nonspecific binding of thrombin to the gold layer occurred since both sensing and reference regions were backfilled with PEG, as described in the Materials and Methods section. Figure 2D shows the experimental results for reference and sensing resonances. The wavelength shift of the sensing resonance was caused by surface binding events between thrombin molecules and aptamers immobilized onto the gold surface and it increased with increasing concentrations of the thrombin in the sample; moreover, it was also affected by the value of the bulk RI, which increases with the thrombin concentration as well. On the other hand, even though the reference region was not functionalized with aptamers, the position of the reference resonance shifted toward longer wavelengths because the bulk RI increased with concentration (light-blue bars). To cancel out the effect of the bulk RI increase and improve the accuracy of the measurement, these data were further processed. First, since the sensitivity of the reference resonance $S_{reference,\ exp}$ is a factor ~2.5 lower than the sensing reference $S_{sensing,\ exp}$, the reference wavelength shift had to be rescaled (i.e., multiplied) of the same quantity. Then, the

https://doi.org/10.1021/acssensors.2c01362
ACS Sens. 2022, 7, 3360−3368

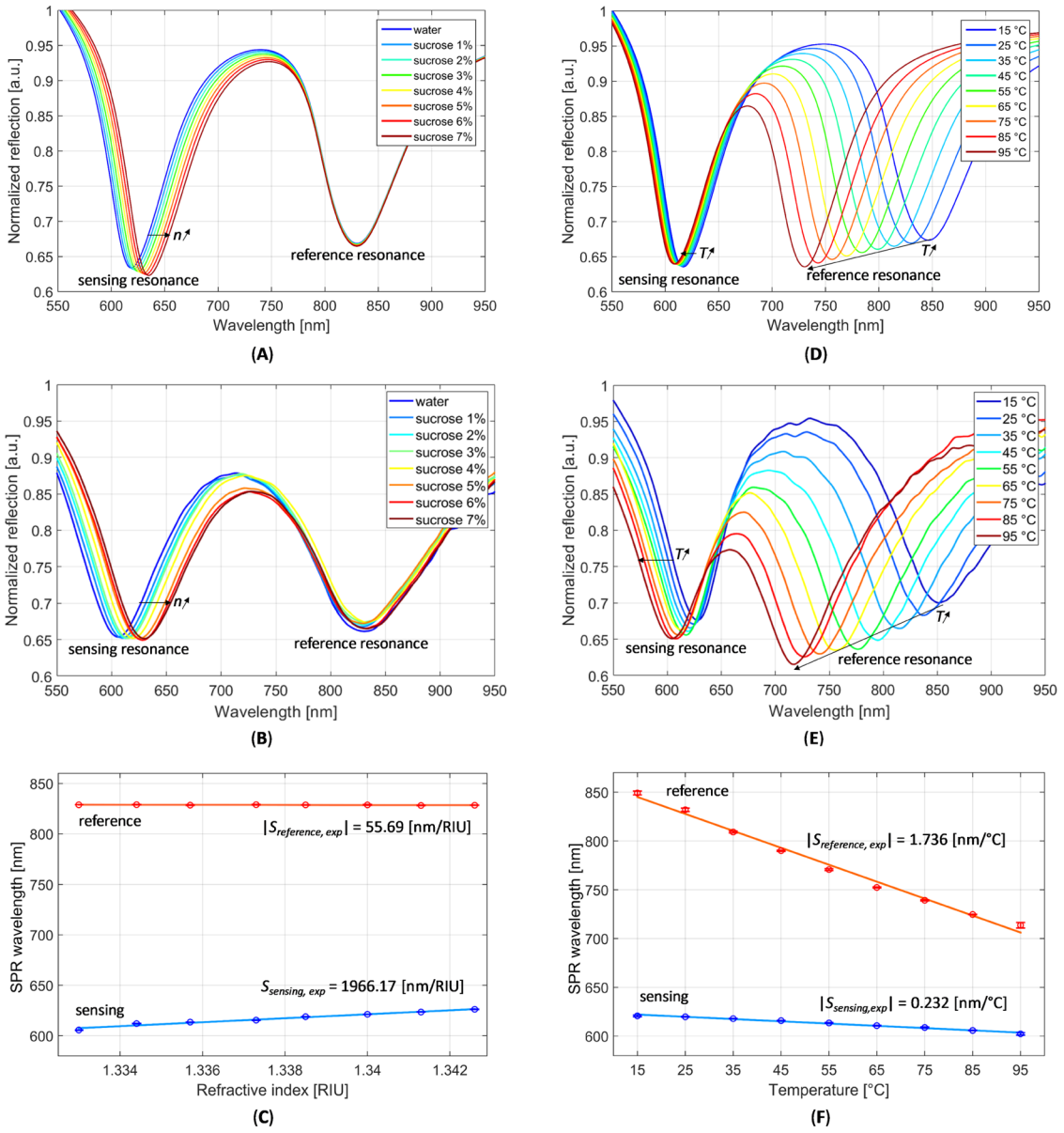

Figure 3. Theoretical and experimental results for the PDMS−gold probe configuration. (A) Theoretical output spectra for increasing RI (n) of the samples: the wavelength position of the reference resonance does not change when the concentration increases. (B) Experimental output spectra for the FO-SPR biosensor dipped in sucrose−water solutions. (C) Experimental linear calibration curves as a function of the RI. Error bars refer to 1 standard deviation (number of samples = 5). (D) Theoretical output spectra for the increasing temperature of the sample (distilled water). (E) Experimental output spectra for the increasing temperature of the sample (distilled water). (F) Experimental linear calibration curves as a function of the temperature. Error bars refer to 1 standard deviation (number of samples = 5).

control signal for the 0 nM concentration was subtracted from the signal obtained for the other concentrations (for both the reference and sensing wavelength shifts, respectively). Eventually, the processed resonance wavelength shifts for the 62, 124, and 248 nm concentration samples were subtracted from the sensing wavelength shifts of the same concentrations, respectively. In this way, the bulk-RI-compensated signal was obtained (green bars of Figure 2D). This wavelength shift does not depend on the bulk RI, but it is only due to surface binding.

Theoretical Investigation and Experimental Testing of PDMS−Gold Probe Configurations. Similarly to what was done for the gold−gold probe configuration, the theoretical behavior of the PDMS−gold probe configuration was studied by simulating its response to a sucrose−water solution series with RIs varying from 1.3330 to 1.3432 RIU. The theoretical spectral response is shown in Figure 3A. The resonance at 610 nm (in water) is ascribed to the sensing region, while the other resonance, produced by the reference region, is located at higher wavelengths (830 nm in water) because the PDMS RI is higher than that of simulated sucrose−water solutions. Moreover, the sensing resonance underwent a red-shift when the sample RI increased, while the position of the reference region stayed constant. This wanted effect occurred because the polymeric layer was thick enough to prevent the evanescent wave generated at the gold interface from reaching the sample under study. The theoretical sensitivities resulted in being $S_{\text{sensing, theor}}$ = 1701.91 nm/RIU and $S_{\text{reference, theor}}$ = 18.36 nm/RIU, with the latter one almost equal to zero since the spectral response of the reference

https://doi.org/10.1021/acssensors.2c01362
ACS Sens. 2022, 7, 3360−3368

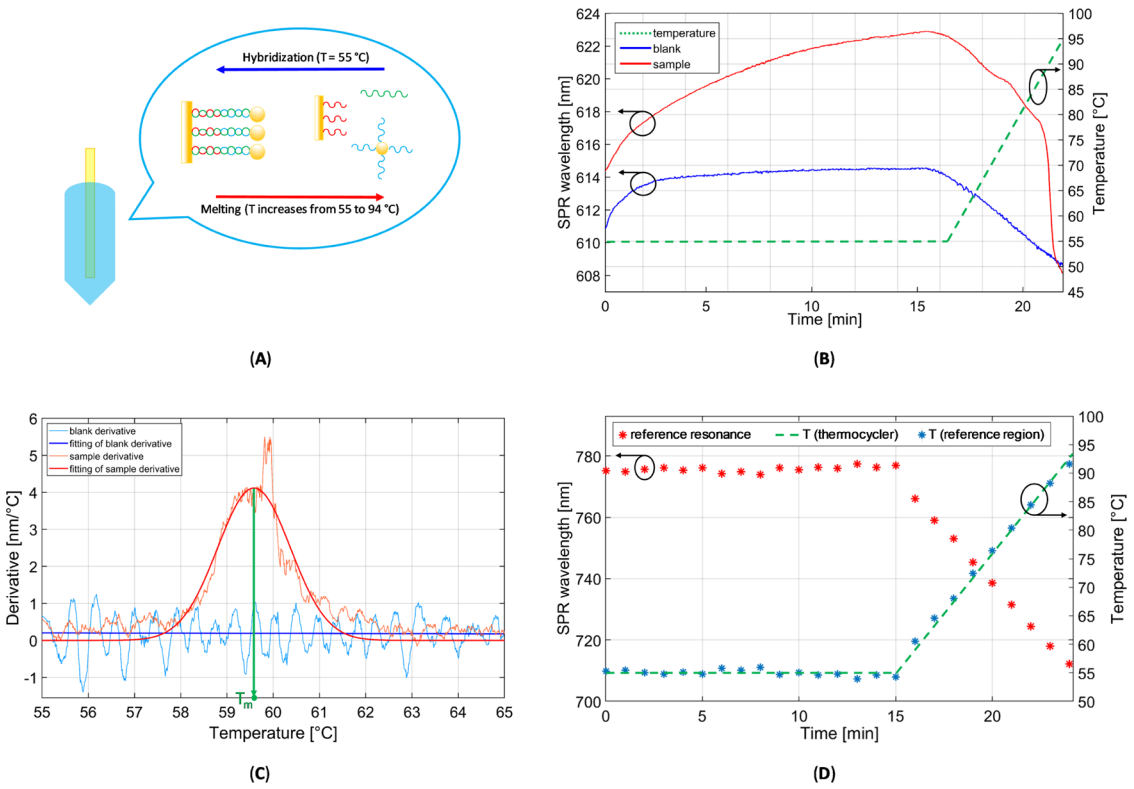

Figure 4. Experimental results of the high-resolution melting assay implemented on the PDMS−gold FO-SPR probe configuration. (A) Schematic illustration of the working principle of the assembly and HRM with gold nanoparticles. (B) Sensorgram of the sensing resonance for the biosensor dipped in the blank solution (blue trace) and in the sample containing the target DNA (red trace). The green trace represents the applied temperature profile over time. (C) Derivative of the sensorgrams for the blank solution (blue trace) and for the target containing the target DNA (red trace). The peak of the red curve allows us to identify the value of the melting temperature T_m. (D) Evolution of the wavelength position of the reference resonance as a function of time and as a consequence of temperature variations (red-starred trace), temperature profile set in the thermocycler (green dashed trace), and actual temperature measured by the reference region (blue starred trace).

region was not expected to change with bulk RI changes. The experimental spectra reported in Figure 3B revealed a good match with the theoretical simulations, as shown by the experimental calibration curves in Figure 3C with sensitivities $S_{sensing,\ exp}$ = 1966.17 ± 0.81 nm/RIU and $|S_{reference,\ exp}|$ = 55.69 ± 0.43 nm/RIU.

Since the main application for this probe configuration is temperature fluctuation monitoring, the theoretical model was applied to investigate the response to temperature variations of deionized water in the range of 15−95 °C. Since both the TOCs of water and PDMS are negative, the two SPR resonances undergo a shift toward shorter wavelengths when the temperature increases (Figure 3D). The theoretical values of sensitivity to temperature variations for the two regions are $S_{sensing,\ theor}$ = 0.172 nm/°C and $S_{refrence,\ theor}$ = 1.559 nm/°C, with the latter being much bigger than the former because the TOC modulus of PDMS is higher than that of water. Afterward, the FO-SPR biosensor was tested in deionized water, heating up the sample with the programmable thermocycler from 15 to 95 °C in steps of 10 °C. The sample was covered by a layer of mineral oil to prevent evaporation. Figure 3E shows that the shape of the experimental spectra is in very good agreement with the theoretical ones. Figure 3F reports the experimental linear calibration curves with sensitivities $|S_{sensing,\ exp}|$ = 0.232 ± 0.015 nm/°C and $|S_{reference,\ exp}|$ = 1.736 ± 0.035 nm/°C. Again, a good match between theoretical and experimental data was observed.

The HRM assay was eventually implemented as a proof of concept. The working principle of the HRM assay is shown in Figure 4A. The whole melting curve assay is described in detail in a previous publication.[38] As described in the Materials and Methods section, the assay was run first in the blank solution and then in the reaction mixture containing the target DNA. Figure 4B reports the temperature profile over time (green dotted line) and the experimental sensorgrams for the sensing resonance. The blue trace is the sensorgram obtained with the FO-SPR biosensor dipped in the blank solution in the absence of target DNA. In principle, any type of binding event can take place at the gold surface. However, the sensing resonance still undergoes wavelength variations due to the temperature changes occurring during the HRM steps. In particular, during the first 2−3 min, the resonance wavelength shows a transient increase that is likely due to a combination of delayed thermal effects from the previous HRM cycle and unwanted bindings occurring between the fiber gold surface and the Au NPs. On the other hand, the red trace is the sensorgram representing the shift taking place in the sensing region during the measurements carried out in the sample containing the target DNA. In this case, the SPR signal strongly increases during the hybridization at a constant temperature of 55 °C. The shift is caused by the single-stranded DNA target molecules that bind simultaneously to the Au NPs and to the gold surface of the optical fiber. In the following step, the sample is slowly heated up to 94 °C. The surface-bound DNA starts melting, and the NPs detach from the probe surface causing a blue-shift of the

https://doi.org/10.1021/acssensors.2c01362
ACS Sens. 2022, 7, 3360−3368

SPR wavelength. In correspondence of the melting temperature (T_m), the sensorgram exhibits an inflection point that can be better recognized by computing the first derivative of the signal with respect to temperature (Figure 4C) and fitting it with a Gaussian function. The obtained result is $T_m = 61.3 \pm 1.5$ °C (with five repetitions of the experiment), in agreement with the value obtained in previous experiments carried out on single-region FO-SPR biosensors.[37] Figure 4D reports the results obtained for the reference resonance when the biosensor is dipped in the sample containing the DNA target, in comparison with the temperature profile set in the thermocycler (green dashed trace). Here, the resonance position (red-starred trace) is only determined by the thermal effects on the PDMS layer. Indeed, it is constant during the hybridization at a constant temperature and then it starts decreasing during the transition from 55 to 94 °C, in agreement with the simulations and with the testing carried out in water at different temperatures. Thus, the reference region could be used to monitor the temperature variations during the HRM assay, in principle, without using the external thermocouple in the thermocycler. Hence, by inverting the equation of the experimental calibration curve (SPR wavelength of reference resonance = $-1.736 \cdot T + 871.06$; Figure 3F), the actual temperature measured by the reference region was retrieved (blue starred trace). Showing only very small fluctuations, it is in substantial agreement with the green dashed trace, meaning that the actual temperature well follows the temperature profile set in the thermocycler.

CONCLUSIONS

In this work, a dual-region self-referencing FO-SPR biosensor was theoretically designed, fabricated, and validated with real bioassays. Two different FO-SPR probe configurations were presented to realize a biosensor capable of compensating and correcting for bulk RI variations or temperature oscillations. The performances of the two probe configurations were simulated employing a theoretical model purposely implemented. The gold−gold configuration, constituted by two separate regions with different lengths and coated by gold layers of different thicknesses, showed sensitivities up to 1653.86 nm/RIU, which are in good agreement with the theoretical predictions. Furthermore, this configuration was successfully employed in a bioassay for thrombin detection, proving the feasibility of functionalizing only the sensing regions and using the reference region to measure bulk RI variations. In the PDMS−gold configuration, the reference zone was coated with an extra PDMS layer. Thanks to the high TOC of PDMS, this configuration turned out to be particularly suitable to monitor signal variations caused by temperature fluctuations. Tests in distilled water with temperatures varying from 15 to 95 °C revealed a sensitivity to temperature for the reference region equal to 1.736 nm/°C. Eventually, an HRM assay with the use of Au NPs for signal amplification was carried out using this second configuration. It was demonstrated that it is possible to correctly determine the melting temperature of the target DNA sequence and independently measure the temperature profile changes occurring during the HRM analysis using the reference zone of the fiber itself, without using an external in situ temperature sensor and by exploiting the same detection technique. In this way, it is possible to have a very accurate and reliable match between the sensorgram of the reaction and the temperature evolution for every time instant. Moreover, since the volume of fluid used for the test is very small (~500 μL), inserting an external sensor inside the vial containing the liquid might be very bulky and inconvenient. The results presented in this paper are very promising since, to the best of the authors' knowledge, they represent one of the first successful examples of dual-region self-referencing FO-SPR biosensors successfully employed to carry out biological analyses. In particular, for the first time, in this work DNA bioassays were performed on FO-SPR biosensors provided also with a region for autonomous and simultaneous integrated temperature control.

ASSOCIATED CONTENT

Supporting Information

The Supporting Information is available free of charge at https://pubs.acs.org/doi/10.1021/acssensors.2c01362.

Design and implementation of a dual-region fiber-optic surface plasmon resonance biosensor; detailed description of the theoretical model; analysis of the variability of the biosensor design parameters; study of variability of the performances; and results of theoretical simulations (PDF)

AUTHOR INFORMATION

Corresponding Author

Jeroen Lammertyn − *MeBioS-Biosensor Group, Faculty Bioscience Engineering, Department of Biosystems, KU Leuven, 3001 Leuven, Belgium;* orcid.org/0000-0001-8143-6794; Email: jeroen.lammertyn@kuleuven.be

Authors

Valentina Bello − *Department of Electrical, Computer and Biomedical Engineering, University of Pavia, 27100 Pavia, Italy; MeBioS-Biosensor Group, Faculty Bioscience Engineering, Department of Biosystems, KU Leuven, 3001 Leuven, Belgium;* orcid.org/0000-0003-3231-0604

Wouter Vandezande − *Centre for Membrane Separations, Adsorption, Catalysis and Spectroscopy for Sustainable Solutions, Department of Microbial and Molecular Systems, KU Leuven, 3001 Leuven, Belgium*

Devin Daems − *MeBioS-Biosensor Group, Faculty Bioscience Engineering, Department of Biosystems, KU Leuven, 3001 Leuven, Belgium*

Complete contact information is available at: https://pubs.acs.org/10.1021/acssensors.2c01362

Notes

The authors declare the following competing financial interest(s): Jeroen Lammertyn is founder and board member of FOx Biosystems, a company commercializing fiber optic SPR technology. He is also (co)-inventor of several patents on this tech-nology.

ACKNOWLEDGMENTS

This work has received funding from European Union's Horizon 2020 research and innovation programme under the Marie Skłodowska-Curie grant agreement No. 955623 (H2020-MSCAITN-CONSENSE).

REFERENCES

(1) Guo, X. Surface Plasmon Resonance Based Biosensor Technique: A Review. *J. Biophotonics* **2012**, *5*, 483−501.

(2) Gopinath, S. C. B. Biosensing Applications of Surface Plasmon Resonance-Based Biacore Technology. *Sens. Actuators, B* **2010**, *150*, 722−733.
(3) Homola, J. Surface Plasmon Resonance Sensors for Detection of Chemical and Biological Species. *Chem. Rev.* **2008**, *108*, 462−493.
(4) Homola, J.; Yee, S. S.; Gauglitz, G. Surface Plasmon Resonance Sensors: Review. *Sens. Actuators, B* **1999**, *54*, 3−15.
(5) Schasfoort, R. B. M.; Richard, B. M. *Handbook of Surface Plasmon Resonance*; Royal Society of Chemistry, 2017.
(6) Homola, J. Present and Future of Surface Plasmon Resonance Biosensors. *Anal. Bioanal. Chem.* **2003**, *377*, 528−539.
(7) Kretschmann, E.; Raether, H. Radiative Decay of Non Radiative Surface Plasmons Excited by Light. *Z. Naturforsch., A: J. Phys. Sci.* **1968**, 2135−2136.
(8) Kretschmann, E. Die Bestimmung Optischer Konstanten von Metallen Durch Anregung von Oberflächenplasmaschwingungen. *Z. Phys.* **1971**, *241*, 313−324.
(9) Otto, A. Excitation of Nonradiative Surface Plasma Waves in Silver by the Method of Frustrated Total Reflection. *Z. Phys.* **1968**, *216*, 398−410.
(10) Pollet, J.; Delport, F.; Janssen, K. P. F.; Jans, K.; Maes, G.; Pfeiffer, H.; Wevers, M.; Lammertyn, J. Fiber Optic SPR Biosensing of DNA Hybridization and DNA−Protein Interactions. *Biosens. Bioelectron.* **2009**, *25*, 864−869.
(11) Knez, K.; Janssen, K. P. F.; Pollet, J.; Spasic, D.; Lammertyn, J. Fiber-Optic High-Resolution Genetic Screening Using Gold-Labeled Gene Probes. *Small* **2012**, *8*, 868−872.
(12) Peeters, B.; Daems, D.; Van der Donck, T.; Delport, F.; Lammertyn, J. Real-Time FO-SPR Monitoring of Solid-Phase DNAzyme Cleavage Activity for Cutting-Edge Biosensing. *ACS Appl. Mater. Interfaces* **2019**, *11*, 6759−6768.
(13) Li, D.; Wu, P.; Zhu, R.; Yang, J.; Yu, H.; Xu, K. In *Implantable Fiber-Optic SPR Sensor Modified with LPFG and PAA-Ran-PAAPBA for Continuous Glucose Monitoring*, 2012 IEEE Sensors; IEEE, 2012.
(14) Liu, F.; Zhang, X.; Li, K.; Guo, T.; Ianoul, A.; Albert, J. Discrimination of Bulk and Surface Refractive Index Change in Plasmonic Sensors with Narrow Bandwidth Resonance Combs. *ACS Sens.* **2021**, *6*, 3013−3023.
(15) Garg, R.; Tripathi, S. M.; Thyagarajan, K.; Bock, W. J. Long Period Fiber Grating Based Temperature-Compensated High Performance Sensor for Bio-Chemical Sensing Applications. *Sens. Actuators, B* **2013**, *176*, 1121−1127.
(16) Hu, T.; Zhao, Y.; Song, A. Fiber Optic SPR Sensor for Refractive Index and Temperature Measurement Based on MMF-FBG-MMF Structure. *Sens. Actuators, B* **2016**, *237*, 521−525.
(17) Weng, S.; Pei, L.; Liu, C.; Wang, J.; Li, J.; Ning, T. Double-Side Polished Fiber SPR Sensor for Simultaneous Temperature and Refractive Index Measurement. *IEEE Photonics Technol. Lett.* **2016**, *28*, 1916−1919.
(18) Velázquez-González, J. S.; Monzón-Hernández, D.; Moreno-Hernández, D.; Martínez-Piñón, F.; Hernández-Romano, I. Simultaneous Measurement of Refractive Index and Temperature Using a SPR-Based Fiber Optic Sensor. *Sens. Actuators, B* **2017**, *242*, 912−920.
(19) Peng, W.; Banerji, S.; Kim, Y.-C.; Booksh, K. S. Investigation of Dual-Channel Fiber-Optic Surface Plasmon Resonance Sensing for Biological Applications. *Opt. Lett.* **2005**, *30*, 2988−2990.
(20) Gong, P.; Wang, Y.; Zhou, X.; Wang, S.; Zhang, Y.; Zhao, Y.; Nguyen, L. V.; Ebendorff-Heidepriem, H.; Peng, L.; Warren-Smith, S. C.; Li, X. In Situ Temperature-Compensated DNA Hybridization Detection Using a Dual-Channel Optical Fiber Sensor. *Anal. Chem.* **2021**, *93*, 10561−10567.
(21) Wu, S.; Tan, Q.; Forsberg, E.; Hu, S.; He, S. In-Situ Dual-Channel Surface Plasmon Resonance Fiber Sensor for Temperature-Compensated Detection of Glucose Concentration. *Opt. Express* **2020**, *28*, 21046−21061.
(22) Wang, Q.; Wang, X. Z.; Song, H.; Zhao, W. M.; Jing, J. Y. A Dual Channel Self-Compensation Optical Fiber Biosensor Based on Coupling of Surface Plasmon Polariton. *Opt. Laser Technol.* **2020**, *124*, No. 106002.
(23) Lu, M.; Peng, W.; Liu, Q.; Liu, Y.; Li, L.; Liang, Y.; Masson, J.-F. Dual Channel Multilayer-Coated Surface Plasmon Resonance Sensor for Dual Refractive Index Range Measurements. *Opt. Express* **2017**, *25*, No. 8563.
(24) Wang, Q.; Song, H.; Zhu, A.; Qiu, F. A Label-Free and Anti-Interference Dual-Channel SPR Fiber Optic Sensor with Self-Compensation for Biomarker Detection. *IEEE Trans. Instrum. Meas.* **2021**, *70*, No. 3039627.
(25) Li, L.; Liang, Y.; Liu, Q.; Peng, W. Dual-Channel Fiber-Optic Biosensor for Self-Compensated Refractive Index Measurement. *IEEE Photonics Technol. Lett.* **2016**, *28*, 2110−2113.
(26) Liu, Z.; Wei, Y.; Zhang, Y.; Wang, Y.; Zhao, E.; Zhang, Y.; Yang, J.; Liu, C.; Yuan, L. A Multi-Channel Fiber SPR Sensor Based on TDM Technology. *Sens. Actuators, B* **2016**, *226*, 326−331.
(27) Liu, L.; Zheng, J.; Deng, S.; Yuan, L.; Teng, C. Parallel Polished Plastic Optical Fiber-Based Spr Sensor for Simultaneous Measurement of Ri and Temperature. *IEEE Trans. Instrum. Meas.* **2021**, *70*, 1−8.
(28) Su, N.; Luo, W.; Wang, L.; Zhang, Z.; Wang, R. A Novel Dual-Wavelength Method for Evaluating Temperature Effect in Fiber-Optic SPR Sensors. *Appl. Sci.* **2021**, *11*, No. 9011.
(29) Zhu, Z.; Liu, L.; Liu, Z.; Zhang, Y.; Zhang, Y. Surface-Plasmon-Resonance-Based Optical-Fiber Temperature Sensor with High Sensitivity and High Figure of Merit. *Opt. Lett.* **2017**, *42*, 2948−2951.
(30) Yeh, P. *Optical Waves in Layered Media*; Wiley, 2005.
(31) Gupta, B. D.; Sharma, A. K. Sensitivity Evaluation of a Multi-Layered Surface Plasmon Resonance-Based Fiber Optic Sensor: A Theoretical Study. *Sens. Actuators, B* **2005**, *107*, 40−46.
(32) Kanso, M.; Cuenot, S.; Louarn, G. Sensitivity of Optical Fiber Sensor Based on Surface Plasmon Resonance: Modeling and Experiments. *Plasmonics* **2008**, *3*, 49−57.
(33) Yuan, Y.; Wang, L.; Huang, J. Theoretical Investigation for Two Cascaded SPR Fiber Optic Sensors. *Sens. Actuators, B* **2012**, *161*, 269−273.
(34) Daems, D.; Pfeifer, W.; Rutten, I.; Saccà, B.; Spasic, D.; Lammertyn, J. Three-Dimensional DNA Origami as Programmable Anchoring Points for Bioreceptors in Fiber Optic Surface Plasmon Resonance Biosensing. *ACS Appl. Mater. Interfaces* **2018**, *10*, 23539−23547.
(35) Li, Y.; Ling, L. Aptamer-Based Fluorescent Solid-Phase Thrombin Assay Using a Silver-Coated Glass Substrate and Signal Amplification by Glucose Oxidase. *Microchim. Acta* **2015**, *182*, 1849−1854.
(36) Pollet, J.; Delport, F.; Janssen, K. P. F.; Tran, D. T.; Wouters, J.; Verbiest, T.; Lammertyn, J. Fast and Accurate Peanut Allergen Detection with Nanobead Enhanced Optical Fiber SPR Biosensor. *Talanta* **2011**, *83*, 1436−1441.
(37) Daems, D.; Peeters, B.; Delport, F.; Remans, T.; Lammertyn, J.; Spasic, D. Identification and Quantification of Celery Allergens Using Fiber Optic Surface Plasmon Resonance PCR. *Sensors* **2017**, *17*, No. 1754.
(38) Daems, D.; Knez, K.; Delport, F.; Spasic, D.; Lammertyn, J. Real-Time PCR Melting Analysis with Fiber Optic SPR Enables Multiplex DNA Identification of Bacteria. *Analyst* **2016**, *141*, 1906−1911.

https://doi.org/10.1021/acssensors.2c01362
ACS Sens. 2022, 7, 3360−3368